International Communications in Heat and Mass Transfer 61 (2015) 16–25

Contents lists available at ScienceDirect

International Communications in Heat and Mass Transfer

journal homepage: www.elsevier.com/locate/ichmt

On characteristics of a non-reacting and a reacting turbulent flow over a backward facing step (BFS)☆

Mina Shahi *, Jim.B.W. Kok, Artur Pozarlik

University of Twente, Faculty of Engineering Technology, Laboratory of Thermal Engineering, Enschede, The Netherlands

ARTICLE INFO

Available online 12 December 2014

Keywords:
Backward facing step
Premixed turbulent combustion
Reacting flow
Non-reacting flow
Numerical model

ABSTRACT

The turbulent reacting flow over a backward facing step shares some essential characteristics of premixed combustion occurring in a typical gas turbine combustor, while it is a simpler configuration to observe and model. For this reason and to explore the characteristics of the turbulent flow, in this study the combustion and flow dynamics in a backward facing step as a most elementary part of a combustor is studied numerically in atmospheric conditions. Two different configurations representing two laboratory devices are considered. As a first necessary step, the accuracy of predicted results is validated through the detailed comparison of numerical predictions and experimental measurements for a non-reacting flow. First, based on these non-reacting calculations, the turbulent model is selected and then the reacting simulations are done using a standard combustion model (available in CFX). Calculations are well supported with experimental data available from literature. Among the investigated turbulence models ($k-\omega$, SST and SAS–SST), SAS–SST model showed the best agreement with the experimental data. The chosen turbulence model was used for the calculation of well documented case of turbulent flow over a backward facing step with the heated wall, showing satisfactory results compared to experimental data. For modeling of the reacting flow, the BVM combustion model was used. The predicted results using this model showed accurate results with an error about 2% on prediction of reattachment length.

1. Introduction

The boundary layer separation of turbulent flow and its subsequent reattachment to a solid surface occurs in many engineering systems, and it has attracted many researchers due to its practical applications. Flows over air foils, in a channel with a sudden area increase, in gas turbines and many heat transfer devices are some of these applications [1–4]. With the abundance of literature and experimental data, the flow past a backward facing step is often used as a benchmark test case for CFD codes and turbulence models. RANS, LES and DNS codes have all been used to simulate this flow in both 2D and 3D domains [3,5–9]. However in the present work, the main goal is to predict the exothermic effects on the flow and the combustion dynamics leading to thermoacoustic instabilities in a backward facing step stabilized premixed flame. The combustor of a typical gas turbine represents some similarities with the turbulent flow over a backward facing step as the flame is stabilized by the recirculating area. Besides, due to the blockage, the sudden expansion also occurs; Regardless of whether these blockages are squares or cylinders, a wake-like flow behind the obstacle will be formed which is characterized by a slow inner flow in the recirculating area and fast outer flow of reactants. This recirculation area plays a critical role to sustain the stable combustion, because it acts as an ignition source for reactants traveling into the shear layer at the edge of the step. Since in many circumstances the occurrence of instability is related to the behavior of this recirculation zone or the wake region during the combustion [10–13], the generated data in the combustible flow over a backward facing step can be used in the subsequent investigation of flame characteristics in more complex configurations of a real gas turbine. To understand the elementary process of interaction between combustion and flow perturbation, it is important to access to comprehensive numerical tools which can carefully take into account all aspects of turbulent combustion flow. Here the backward facing step due to its simple geometry and availability of well documented experimental data is considered for the further investigation. Indeed, the location of the reattachment zone and its flow structure determine the local heat and mass transport properties of the flow. Furthermore the characteristics of backward facing step flow allow to exam several important aspects of turbulent flows. These aspects include separation of a turbulent boundary layer, reattachment of the boundary layer, recirculation, and the occurrence of secondary separation regions, in which the reattachment zone determines the initial conditions for the recovery process downstream of the step. When the fluid flows over a step, the flow separation can cause alternating shedding of vortices from the body, inducing fluctuating forces

☆ Communicated by: W.J. Minkowycz.

* Corresponding author.
E-mail addresses: m.shahi@utwente.nl, mina.shahi@gmail.com (M. Shahi).

http://dx.doi.org/10.1016/j.icheatmasstransfer.2014.11.005
0735-1933/

which may result in structural vibrations and noise. This can even lead to structural failure. This subject has been of great interest and a lot of efforts have been done into studying the size of the recirculating zone under various conditions as well as vortex interactions during blow off or unstable conditions [12,14,15].

As it has been mentioned above in order to assess the available numerical tools, this paper is devoted to characterize the turbulent flow over the backward facing step in two different configurations defined based on the test rigs used by Pitz et al. [16] and Vogel et al. [17]. Prior to the results section, the used numerical approaches are described in detail. Then the mean velocity field of a mixing layer formed at the edge of the step in the first configuration is studied under both reacting and non-reacting conditions; the effectiveness of the used turbulence model on the characteristics of the turbulent flow over the step in the absence of the reaction is discussed. Next, calculations are performed for the reacting flow using the turbulence model, which presented the best agreement with the experiment, together with the Burning Velocity combustion Model (BVM). Thereafter, in the second configuration, the transient heat transfer between the working flow (i.e. air) and the wall is investigated in absence of other complicated processes like combustion, and swirling flow. In this case a heat source is embedded on the wall behind the step. To verify the accurate prediction of the flow and thermal boundary layer, the mean velocity and temperature profiles are compared with the available experimental data; in all calculations, the size of recirculating area is compared to the measurements, giving the good consistency.

2. Problem definition

The schematic of a backward facing step is shown in Fig. 1. The flow coming from the left separates at the sharp corner of the step and then reattaches itself to the lower wall at a distance L, behind the step. A recirculation region is subsequently produced directly behind the step. The reattachment length, L, is a function of the Reynolds number, and the expansion ratio H2:H1 [18]. Depending on the Reynolds number, secondary recirculation regions may occur further downstream past the main recirculation bubble. Flow separation may also occur on the upper wall [18,19].

3. Numerical approach

In this paper, two different configurations are considered for simulations which respectively are chosen in accordance to the experimental setup of Pitz et al. [16] and Vogel et al. [17]. The computational domains consist of unstructured elements. A grid refinement study is performed to determine whether the resolution is accurate enough to capture certain mean flow parameters. The information of the chosen grid is summarized in Table 1. The mesh density is increased in vicinity of the step and walls. The numerical simulations were made here by using ANSYS CFX V12.1. It uses an implicit finite volume formulation to construct the discretized equations representing the Reynolds Averaged Navier–Stokes (RANS)

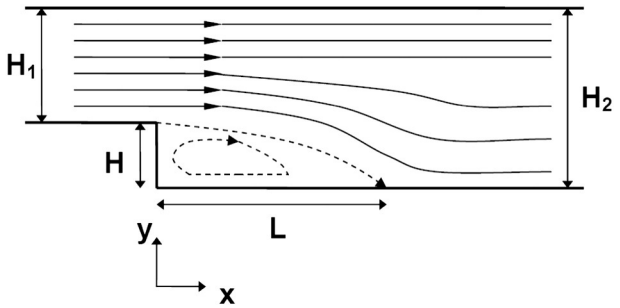

Fig. 1. Geometry and flow pattern for the backward-facing step calculations.

Table 1
Grid information.

	Configuration 1 Pitz et al. [16]	Configuration 2 Vogel et al. [17]
Number of elements	164,785	48,498

equations. The model consists of a compressible solver with a co-located (non-staggered) finite volume method, such that the control volumes are identical for all transport equations [20]. The basic set of balance equations solved by ANSYS CFX comprises the Navier–Stokes, species and energy transport equations which are summarized in the following section. A coupled algebraic multi-grid solver is used to give robust solutions for the governing system of linearized equations representing the differential transport equations in discretized form. Convective terms are discretized using a high resolution scheme. It provides high spectral resolution and both low numerical diffusion and dispersion. While shape functions are used to evaluate spatial derivatives for all the diffusion terms. A second order backward Euler discretization is used for time accuracy. In the time implicit compressible methods, the full compressible equations are solved implicitly to remove the CFL constraint. However to keep the results more precise the solver must be run for constrained CFL values [21]. Therefore the calculations are performed with the time steps (Δt) of 1e − 5 s. Boundary conditions which are selected according to [16] and [17] will be explained later in the respective sections.

4. Mathematical formulation

The full numerical solution of the Navier–Stokes equations is limited to very simple cases, where not a large range of turbulent length and time scales is involved. Therefore to overcome these difficulties, an additional step is introduced by averaging the transport equations. In the Reynolds average, each quantity (ϕ) is split into a mean $\left(\overline{\phi} = {}^{1}/_{T}\int_{T}\phi(t)dt\right)$ and a deviation from mean (turbulent fluctuating component) denoted by ($\phi' = \phi - \overline{\phi}$). The Favre average is defined as the density-weighted average by which the flow variables will be decomposed into mean, $\widetilde{\phi} \equiv \overline{\rho\phi}/\rho$, and fluctuating parts, $\phi'' \equiv \phi - \widetilde{\phi}$. After time-averaging the equations, extra terms appear in the flow equations which are associated with the interactions between various turbulent fluctuations [22]. Decomposing the velocity, u_i, total energy (non-chemical) e_0 and chemical species Y_k into their Favre average and the corresponding fluctuations and taking the Reynolds average of the conservation equations gives:

– Conservation of mass

$$\frac{\partial\overline{\rho}}{\partial t} + \frac{\partial(\overline{\rho}\widetilde{u}_i)}{\partial x_i} = 0. \tag{1}$$

– Momentum

$$\frac{\partial(\overline{\rho}\widetilde{u}_i)}{\partial t} + \frac{\partial\left(\overline{\rho}\widetilde{u}_i\widetilde{u}_j\right)}{\partial x_i} = -\frac{\partial\overline{p}}{\partial x_i} + \frac{\partial}{\partial x_i}\left(\overline{\tau}_{ij} - \overline{\rho u_i'' u_j''}\right) \tag{2}$$

τ is the stress tensor which is related to the strain rate by:

$$\overline{\tau}_{ij} = \widetilde{\tau}_{ij} + \overline{\tau}_{ij}'' \tag{3}$$

– Chemical species

$$\frac{\partial\left(\overline{\rho}\widetilde{Y}_k\right)}{\partial t} + \frac{\partial\left(\overline{\rho}\widetilde{Y}_k\widetilde{u}_i\right)}{\partial x_i} = -\frac{\partial\left(\overline{\rho u_i''\widetilde{Y}_k''}\right)}{\partial x_i} - \frac{\partial\left(\overline{V_{k,i}Y_k}\right)}{\partial x_i} + \overline{\dot{\omega}}_k. \tag{4}$$

The source term in the species transport equations is shown by $\dot{\omega}_k$; V_k is the diffusive velocity of the kth species.

– Energy equation

$$\frac{\partial(\overline{\rho}\widetilde{e_0})}{\partial t}+\frac{\partial}{\partial x_j}\left(\overline{\rho}\widetilde{u}_i\widetilde{e_0}+\widetilde{u}_j\overline{p}+\overline{u_j''p}+\overline{\rho u_j''e_0''}+\overline{q}_j-\overline{u_i\tau_{ij}}\right)=\overline{\dot{\omega}}_T \tag{5}$$

$\overline{\dot{\omega}}_T$ is a chemical source term, and $\widetilde{e_0}$ is given by:

$$\widetilde{e_0}\equiv\widetilde{e}+\widetilde{u}_k\widetilde{u}_k/2+k \tag{6}$$

q_j is the heat flux which represents heat conduction and transport through species gradients given by $\left(q_j=-\lambda\frac{\partial T}{\partial x_j}+\rho\sum_{k=1}^{N}V_{k,j}Y_kh_{s,k}\right)$. The turbulent energy, k, is defined by:

$$k=\frac{\widetilde{u_k''u_k''}}{2}. \tag{7}$$

The objective of turbulent combustion modeling is to propose closures for the unknown quantities (e.g. $\overline{\rho u_i''u_j''}$, $\overline{\rho u_i''Y_k''}$ and $\overline{\rho u_i''h_k''}$). Species fluxes, $\overline{\rho u_i''Y_k''}$, and enthalpy turbulent fluxes, $\overline{\rho u_i''h_k''}$, are generally closed with the use of the classical gradient assumption using a classical gradient assumption.

4.1. Turbulence modeling

In this work in order to describe the highly turbulent reactive flow behavior, k − ω [23,24], SST [25] and SAS–SST [26] turbulent models are implemented.

4.1.1. k – ω turbulence model

The k – ω model [23], was developed to improve the predictions in the near wall region and reduce the errors in adverse pressure gradient calculations. The major advantage of the k–ω model is the robust and elegant way how the near wall region is handled. In order to define the turbulent eddy viscosity, the k–ω model uses a frequency scale (ω) called also specific turbulent dissipation rate. Both turbulent kinetic energy (k) and specific dissipation rate (ω) are obtained from the solution of the following transport equation:

$$\frac{\partial}{\partial t}(\overline{\rho}k)+\frac{\partial}{\partial x_i}(\overline{\rho}\widetilde{u}_ik)=\frac{\partial}{\partial x_i}\left[\left(\mu+\sigma_k\frac{\overline{\rho}k}{\omega}\right)\frac{\partial k}{\partial x_i}\right]+P_k-\beta^*\overline{\rho}k\omega \tag{8}$$

$$\frac{\partial}{\partial t}(\overline{\rho}\omega)+\frac{\partial}{\partial x_i}(\overline{\rho}\widetilde{u}_i\omega)=\frac{\partial}{\partial x_i}\left[\left(\mu+\sigma_\omega\frac{\overline{\rho}k}{\omega}\right)\frac{\partial\omega}{\partial x_i}\right]+a\frac{\omega}{k}P_k-\beta\overline{\rho}\omega^2+\frac{\overline{\rho}\sigma_d}{\omega}\frac{\partial k}{\partial x_i}\frac{\partial\omega}{\partial x_i} \tag{9}$$

where

$$P_k=\tau_{ij}\frac{\partial\widetilde{u}_i}{\partial x_j} \tag{10}$$

$$\tau_{ij}=2\mu_t\widetilde{S}_{ij}-\frac{2}{3}\overline{\rho}k\delta_{ij} \tag{11}$$

$$\widetilde{S}_{ij}=\frac{1}{2}\left(\frac{\partial\widetilde{u}_i}{\partial x_j}+\frac{\partial\widetilde{u}_j}{\partial x_i}\right)-\frac{1}{3}\frac{\partial\widetilde{u}_k}{\partial x_k}\delta_{ij} \tag{12}$$

The eddy viscosity in this model is defined as Eq. (13).

$$\mu_t=\overline{\rho}\frac{k}{\hat{\omega}} \tag{13}$$

where $\hat{\omega}=\max\left[\omega,\ C_{lim}\sqrt{\frac{\widetilde{S_{ij}}\widetilde{S_{ij}}}{\beta^*}}\right]$. β^*, α, β, σ_k, σ_d, σ_ω and C_{lim} are constants or auxiliary functions which are given in [23].

4.1.2. The SST (shear stress transport) Turbulence Model

The $k-\varepsilon$ model has two main weaknesses which are: over predicting the shear stress in adverse pressure gradient flows due to too low dissipation and requirement for near wall modification. The $k-\omega$ model is better in predicting adverse pressure gradient flow and it does not use any damping functions. However it is dependent on the value of ω in free stream flow. In order to improve these models, the SST model suggested by Menter [25] was developed. The SST is an eddy-viscosity model which is using a combination of $k-\varepsilon$ and $k-\omega$ models for the core flow and boundary layer, respectively. For this a blending function F1 is introduced which is equal to one in the near wall region and equal to zero for the flow domain in the outer region. It smoothly switches from the $k-\omega$ model in the near wall region to the $k-\varepsilon$ model for the rest of the flow. In this way, the near-wall performance of the k − ω model can be used without the potential errors resulting from the free stream sensitivity of that model. The modeled equations for the turbulent kinetic energy k and the turbulence frequency ω can be written as follows:

$$\frac{\partial\overline{\rho}k}{\partial t}+\frac{\partial\overline{\rho}\widetilde{u}_jk}{\partial x_j}=\left(2\mu_t\widetilde{S}_{ij}-\frac{2}{3}\overline{\rho}k\delta_{ij}\right)\frac{\partial\widetilde{u}_i}{\partial x_j}-\beta^*\overline{\rho}\omega k+\frac{\partial}{\partial x_j}\left((\mu+\sigma_k\mu_t)\frac{\partial k}{\partial x_j}\right) \tag{14}$$

$$\frac{\partial\overline{\rho}\omega}{\partial t}+\frac{\partial\overline{\rho}\widetilde{u}_j\omega}{\partial x_j}=\frac{\gamma}{v_t}\left(2\mu_t\widetilde{S}_{ij}-\frac{2}{3}\overline{\rho}k\delta_{ij}\right)\frac{\partial\widetilde{u}_i}{\partial x_j}-\beta\overline{\rho}\omega^2+\frac{\partial}{\partial x_j}\left((\mu+\sigma_\omega\mu_t)\frac{\partial\omega}{\partial x_j}\right)+(1-F_1)2\overline{\rho}\sigma_{\omega2}\frac{1}{\omega}\frac{\partial k}{\partial x_j}\frac{\partial\omega}{\partial x_j}. \tag{15}$$

Each of the constants is blend of an inner (1) and outer (2) constant as:

$$\varnothing=F_1\varnothing_1+(1-F_1)\varnothing_2 \tag{16}$$

where $\varnothing_1$ stands for constant 1 and $\varnothing_2$ represents constant 2 (e.g. $\sigma_\omega=F_1\sigma_{\omega1}+(1-F_1)\sigma_{\omega2}$).

Additional functions can be obtained from:

$$F_1=\tanh\left(\arg_1^4\right) \tag{17}$$

$$\arg_1=\min\left(\max\left(\frac{\sqrt{k}}{\beta^*\omega y},\frac{500v}{y^2\omega}\right),\frac{4\rho\sigma_{\omega2}k}{CD_{k\omega}y^2}\right) \tag{18}$$

$$CD_{k\omega}=\max\left(2\overline{\rho}\sigma_{\omega2}\frac{1}{\omega}\frac{\partial k}{\partial x_j}\frac{\partial\omega}{\partial x_j},1.0e{-}10\right) \tag{19}$$

$$\mu_t=\min\left[\frac{\overline{\rho}k}{\omega},\frac{a_1\overline{\rho}k}{SF_2}\right] \tag{20}$$

ρ is density, μ_t is the turbulent viscosity, μ is the molecular dynamic viscosity, y is the distance from the field point to the nearest wall, and S is the vorticity magnitude.and the blending function F_2 can be obtained from:

$$F_2=\tanh\left(\arg_2^2\right) \tag{21}$$

$$\arg_2=\max\left(\left(\frac{2\sqrt{k}}{\beta^*\omega y},\frac{500\widetilde{v}}{y^2\omega}\right)\right) \tag{22}$$

$$\gamma_1 = \frac{\beta_1}{\beta^*} - \frac{\sigma_{\omega 1}\lambda^2}{\sqrt{\beta^*}}\ ,\ \gamma_2 = \frac{\beta_2}{\beta^*} - \frac{\sigma_{\omega 2}\lambda^2}{\sqrt{\beta^*}}. \tag{23}$$

The constants are taken from the ref. [25]:

$$\beta^* = 0.09, a_1 = 0.31, \lambda = 0.41$$

$$\beta_1 = 0.075, \sigma_{\omega 1} = 0.5, \sigma_{k1} = 0.85$$

$$\beta_2 = 0.0828, \sigma_{\omega 2} = 0.856, \sigma_{k2} = 1.0.$$

4.1.3. The SAS turbulence model

The Scale-Adaptive Simulation (SAS) is an advanced URANS model which allows better resolution of the turbulent spectrum in unstable flow conditions. This model can change smoothly between LES-like behavior in regions where the turbulence structure is well resolved and the SST model where the unsteady flow is not well resolved. The starting point of the transformation to the SST model is the k − νt formulation as given by Menter et al. [26].

The following equations have been derived there for the variables k and $\Phi = \sqrt{k}L$:

$$\frac{\partial \bar{\rho} k}{\partial t} + \frac{\partial \tilde{u}_j \rho k}{\partial x_j} = P_k - c_\mu^{\frac{3}{4}} \bar{\rho} \frac{k^2}{\Phi} + \frac{\partial}{\partial y}\left[\frac{\mu_t}{\sigma_k}\frac{\partial k}{\partial y}\right] \tag{24}$$

$$\frac{\partial \bar{\rho} \Phi}{\partial t} + \frac{\partial u_j \bar{\rho} \Phi}{\partial x_j} = \zeta_1 \frac{\Phi}{k} P_k - \zeta_2 \mu_t S \left|u''\right| \frac{\Phi^2}{k^{3/2}} - \zeta_3 \bar{\rho} k + \frac{\partial}{\partial y}\left[\frac{\mu_t}{\sigma_\phi}\frac{\partial \Phi}{\partial y}\right] \tag{25}$$

$$P_k = \nu_t S^2, \nu_t = c_\mu^{1/4}\Phi \tag{26}$$

with

$$\left|u''\right| = \sqrt{\frac{\partial^2 \tilde{u}_i}{\partial x_j^2}\frac{\partial^2 \tilde{u}_i}{\partial x_j^2}} \tag{27}$$

where S is the absolute value of strain rate. Constant used in the SAS model (i.e. ζ_1, ζ_2, ζ_3, cμ and) are given in [24].

Indeed these formulations, contrary to standard URANS models, provide a turbulent length scale, which is proportional to the local flow structure and not to the thickness of the turbulent layer. Since the second derivative term, |**u**″|, in the equation for **Φ** is the SAS-relevant term, the length scale predicted by the above model is largely proportional to the von Karman length scale as:

$$L_{vK} = \kappa \left| \frac{\frac{\partial \tilde{u}}{\partial y}}{\frac{\partial^2 \tilde{u}}{\partial y^2}} \right|. \tag{28}$$

The L_{vK} adjusts to the already resolved scales in a simulation and provides a length-scale, proportional to the size of the resolved eddies.

In order to add the SAS capability into the SST model, the **Φ**-equation is transformed to the **k** − **ω** framework using this relation: $= \frac{1}{c_\mu^{1/4}} \frac{k}{\omega}$.

The resulting ω-equation is:

$$\begin{aligned}\frac{\partial \bar{\rho} \Phi}{\partial t} + \frac{\partial \bar{\rho} \tilde{u}_j \omega}{\partial t} = \alpha \bar{\rho} S^2 - \beta \bar{\rho} \omega^2 + \frac{\partial \omega}{\partial x_j}\left(\frac{\mu_t}{\sigma_\omega}\frac{\partial \omega}{\partial x_j}\right) + \frac{2\bar{\rho}}{\sigma_\Phi}\left(\frac{1}{\omega}\frac{\partial k}{\partial x_j}\frac{\partial \omega}{\partial x_j} - \frac{k}{\omega^2}\frac{\partial \omega}{\partial x_j}\frac{\partial \omega}{\partial x_j}\right) \\ + \tilde{\xi}_2 \bar{\rho} \kappa S^2 \frac{L}{L_{vK}} + \left[\frac{\bar{\rho}\omega}{k}\frac{\partial}{\partial x_j}\left(\frac{\nu_t}{\sigma_\omega}\frac{\partial k}{\partial x_j}\right)\left(\frac{1}{\sigma_k} - \frac{1}{\sigma_\Phi}\right)\right].\end{aligned} \tag{29}$$

The first three terms, on the RHS of the Eq. (29), are the standard terms of the original Wilcox model. The second term, $\frac{2\bar{\rho}}{\sigma_\Phi}\left(\frac{1}{\omega}\frac{\partial k}{\partial x_j}\frac{\partial \omega}{\partial x_j}\right)$, is the cross diffusion term, which is also included in the SST model helping

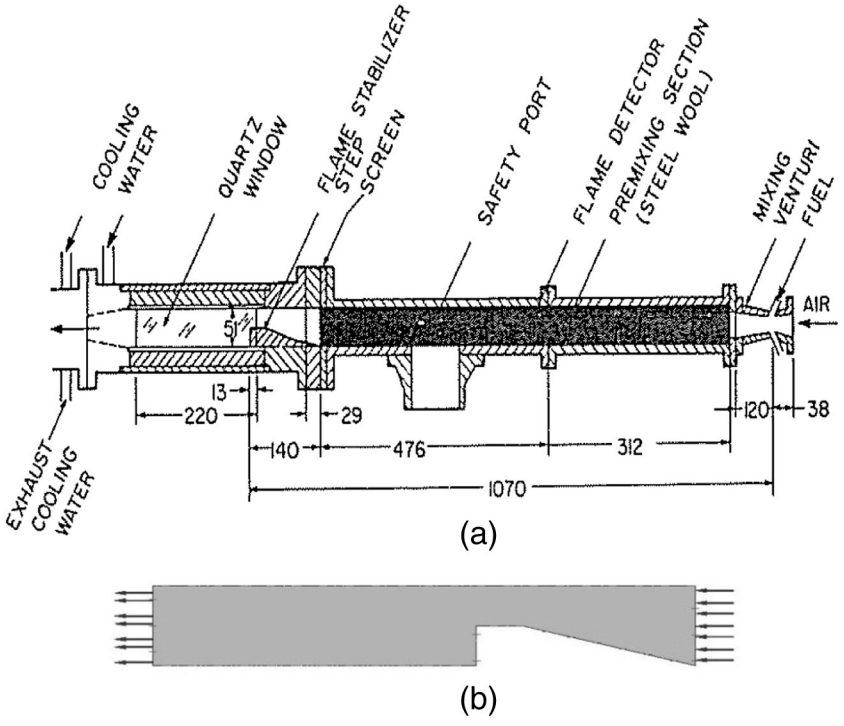

Fig. 2. (a) The experimental set up (from [16]) (b) simplified CFD domain including the flame stabilizer step (i.e. configuration 1).

to prevent the free stream sensitivity. The last term including $\left(\frac{1}{\sigma_k}-\frac{1}{\sigma_\Phi}\right)$ is equal to 0. The remaining term is the $F_{SST-SAS}$ term, $\frac{-2\overline{\rho}}{\sigma_\Phi}\left(\frac{k}{\omega^2}\frac{\partial\omega}{\partial x_j}\frac{\partial\omega}{\partial x_j}\right)+\widetilde{\xi}_2\overline{\rho}\kappa S^2\frac{L}{L_{vK}}$, which is meant to preserve the SST model in the RANS regime and to activate the SAS capability in the URANS regions. This term is modeled as follows:

$$F_{SST\text{-}SAS}=\overline{\rho}F_{SAS}\max \times\left[\widetilde{\xi}_2\kappa S^2\frac{L}{L_{vK}}-\frac{2}{\sigma_\Phi}k\cdot\max\left[\frac{1}{\omega^2}\left(\frac{\partial\omega}{\partial x_j}\frac{\partial\omega}{\partial x_j}\right),\frac{1}{k^2}\frac{\partial k}{\partial x_j}\frac{\partial k}{\partial x_j}\right],0\right] \tag{30}$$

F_{SAS}, $\widetilde{\xi}_2$, and σ_Φ are the constants value.

4.2. Combustion model

The full numerical simulation of a combusting turbulent flow field without any assumptions is still not feasible. Due to limitations of the code and hardware (computational expense), the simulations have been carried out with the help of the Burning Velocity Model (BVM) model which is standard available in the ANSYS CFX code. The basic principles and features of this model are discussed below [27–29]:

4.2.1. Burning velocity model

In premixed and partially premixed flames, the flamelets have a discontinuity between the burnt and the un-burnt regions; to analyze these kinds of flames, two important scalar variables (a mixture fraction and a progress variable) have been introduced which are defined in terms of a normalized fuel mass fraction. In this model the scalar reaction progress variable subdivides the flow field in two different areas, the burnt and the un-burnt mixture. Unlike the reactant and product mass fractions which vary continuously through the field, the progress variable as a convenient marker for both premixed and non-premixed zones is constrained to take values close to zero or unity everywhere except in the flamelets. Therefore burnt regions are treated similar to a diffusion flame whereas the un-burnt region is represented by the cold mixture. The mass fractions in the non-reacted fraction of the fluid, $Y_{i,fresh}$, are obtained by linear blending of fuel and oxidizer compositions. The species mass fractions in the burned fraction of the fluid, $Y_{i,burned}$, are computed by applying the flamelet model.

If a simple global reaction rate mechanism can be assumed, and ignoring the pressure variation, the thermochemistry of premixed combustion can be described in terms of two composition variables (e.g. mixture fraction $Z(x, t)$ and a reactant/product mass fraction $Y_i(x, t)$):

$$\frac{\partial(\rho Z)}{\partial t}+\nabla.(\rho uZ)=\nabla.(\rho D\nabla Z), \tag{31}$$

$$\frac{\partial(\rho Y_i)}{\partial t}+\nabla.(\rho uY_i)=\nabla.(\rho D\nabla Y_i)+\dot{\omega}_i. \tag{32}$$

$D(x, t)$ is the molecular diffusion coefficient, which is assumed to be applicable for all species. These two equations are applicable irrespective of whether combustion takes place premixed, partially premixed or non-premixed flames. However it is more convenient to replace the Y_i by a normalized quantity (i.e. progress variable $c(x, t)$), which is defined as:

$$Y_i(x,t)=Y_i(c(x,t),Z(x,t)) \tag{33}$$

where $c(x, t) = 0$ in reactants and $c(x, t) = 1$ in equilibrium combustion products. By substitution of Eq. (33) into Eq. (32) the instantaneous equation can be written as:

$$\frac{\partial(\rho c)}{\partial t}+\nabla\cdot(\rho uc)=\nabla\cdot(\rho D\nabla c)+\frac{1}{\partial\rho Y_i/\partial c}\cdot\left[\dot{\omega}_i+\frac{\partial^2Y_i}{\partial c^2}\rho\chi_c+\frac{\partial^2Y_i}{\partial Z^2}\rho\chi_Z+\frac{\partial^2Y_i}{\partial c\partial Z}\rho\chi_{Z,c}\right]. \tag{34}$$

The dependency of Y_i and Z leads to the appearance of three additional terms which will be absent in the fully premixed case. These terms contain the following scalar dissipation quantities:

$$\chi_Z=D\nabla Z\cdot\nabla Z \tag{35}$$

$$\chi_c=D\nabla c\cdot\nabla c \tag{36}$$

$$\chi_{Z,c}=D\nabla Z\cdot\nabla c. \tag{37}$$

Eq. (34) can be applied for the all modes of combustion, while without the above mentioned scalar dissipation terms it is only applicable for the fully premixed combustion. The correct consideration for the partially premixed and non-premixed modes is dependent on the dissipation terms. More detailed information about the chemical and molecular terms in the transport equations is given in [29].

For use in Favre-averaged turbulent combustion simulations, the scalars have to be Favre-averaged. As explained before, at any given time and position in space the fluid is considered to be either fresh materials or fully reacted. Then, the averaged reaction progress variable, $\widetilde{c}$, is the probability for the instantaneous state of the fluid being reacted. The mean species composition of the fluid is computed according to:

$$\widetilde{Y}_i=(1-\widetilde{c})\widetilde{Y}_{i,fresh}+\widetilde{c}\widetilde{Y}_{i,burned} \tag{38}$$

and

$$\widetilde{F}=\widetilde{Z}\cdot(1-\widetilde{c}) \tag{39}$$

where F and Z are the weighted reaction progress and mixture fraction, respectively.

The reaction progress variable is computed from the following transport equation:

$$\frac{\partial(\overline{\rho}\widetilde{c})}{\partial t}+\frac{\partial\left(\overline{\rho}\widetilde{u}_j\,\widetilde{c}\right)}{\partial x_j}=\frac{\partial}{\partial x_j}\left[\left(\overline{\rho D}+\frac{\mu_t}{\sigma_F}\right)\frac{\partial\widetilde{c}}{\partial x_j}\right]+\overline{\omega}_c. \tag{40}$$

The weighted reaction progress variable is computed by solving a transport equation:

$$\frac{\partial\left(\overline{\rho}\widetilde{F}\right)}{\partial t}+\frac{\partial\left(\overline{\rho}\widetilde{u}_j\,\widetilde{F}\right)}{\partial x_j}=\frac{\partial}{\partial x_j}\left[\left(\overline{\rho D}+\frac{\mu_t}{\sigma_F}\right)\frac{\partial\widetilde{F}}{\partial x_j}\right]+2\left(\overline{\rho D}+\frac{\mu_t}{\sigma_F}\right)\left(\frac{\partial\widetilde{Z}}{\partial x_j}\cdot\frac{\partial\widetilde{c}}{\partial x_j}\right)-\widetilde{Z}\overline{\omega}_c. \tag{41}$$

The default value of the turbulent Schmidt number for the weighted reaction progress variable is $\sigma_F = 0.9$.

The burning velocity model (BVM) is used to close the combustion source term for reaction progress.

$$\overline{\omega}_c=\overline{S}_c-\frac{\partial}{\partial x_j}\left((\overline{\rho D})\frac{\partial\widetilde{c}}{\partial x_J}\right) \tag{42}$$

$$\overline{S}_c=\overline{\rho}_u S_T|\nabla\widetilde{c}| \tag{43}$$

where $\overline{\rho}_u$ is the density of the unburnt mixture. The diffusive exchange of species and energy, which makes the flame proceed in space, is already accounted for by the source term $\overline{S}_c$. the turbulent burning velocity is calculated using the Zimont model [27].

5. Results and discussion

5.1. Configuration 1: backward facing step according to Pitz and Daily set up

This test case deals with the turbulent premixed propane/air flame stabilized at a backward facing step which has been studied experimentally by Pitz et al. [16]. The test rig is shown in Fig. 2. The air and propane are combined using three parallel venturi tubes and then mixed in a one meter long premixed section. The flow converges over the backside of the profile step with a 2:1 area ratio. The premixed flame is stabilized in a turbulent mixing layer at the edge of a 25 mm high step. The geometry shown in Fig. 2, is completely described in [16]. Here, the simulations are performed for the non-reacting ($\phi = 0$) and reacting ($\phi = 0.57$) premixed propane/air flow at a Reynolds number equal to 22,000. The Reynolds number ($Re_h = \frac{U_0 H}{\upsilon}$) is defined based on the step height, H, average inlet velocity, U_0, and kinetic viscosity, υ. The chosen computational domain which excludes the premixed section is 347 mm long, 51 mm high and has a third dimension in a span-wise direction with a thickness equal to the size of one numerical element. The velocity field at the inlet is specified as that of a fully-developed turbulent channel flow at the equivalent Reynolds number. A pressure-based outlet boundary condition is used for the outflow. The other boundaries are considered as adiabatic and no-slip velocity boundary conditions, whereas the side walls are symmetric.

For the presentation of the results we first start with the general description of the two-dimensional flow field presented for a non-reacting condition. Calculations are done by using various turbulence models. The issues related to each model are addressed and the best model is selected for the further calculations. The reacting case is next simulated by using the chosen turbulence model from previous calculations. Fig. 3 compares the results for velocity profile at the step (i.e. X/H = 0) and X/H = 3 for non-reacting flow. Here, three different turbulence models are used. Numerical predictions of streamwise mean velocity using various turbulence models show a similar trend of flow over the step. The velocity profiles indicate that the flow separated at the step, resulting in recirculation regions behind the step, and then redeveloped along the channel which agrees well with the experimental results. The turbulence model which gave the best prediction in the non-reacting configuration is SAS–SST, while there is still some tendency to over-predict the velocity. Furthermore, the size of the mean recirculation region can be used as a comparative tool for determining the accuracy of backward facing step computations. The size of the recirculation vortex is defined by the reattachment length, L, which is the distance from the step face to the point of zero wall shear stress. It can be also estimated from the velocity field. The predicted value of the reattachment length is reported in Table 2. The SST turbulence model predicted the reattachment length with an error as small as about 5%. More significant error is observed for the $k-\omega$ model with the predicted reattachment length at the position of 6.54 H. While the predicted mean reattachment point by using the SAS–SST model is computed to 6.78 H which gives just about 3% deviation from the measured value of 7H.

To assess the effect of the combustion processes on the mean flow field, transient average stream-wise velocity profiles for the reacting flow are presented in Fig. 4 at three different sections using the BVM combustion model. BVM uses a RIF flamelet library [27] for the 'burnt' mixture; this mechanism involves a 35 species 108 reactions scheme

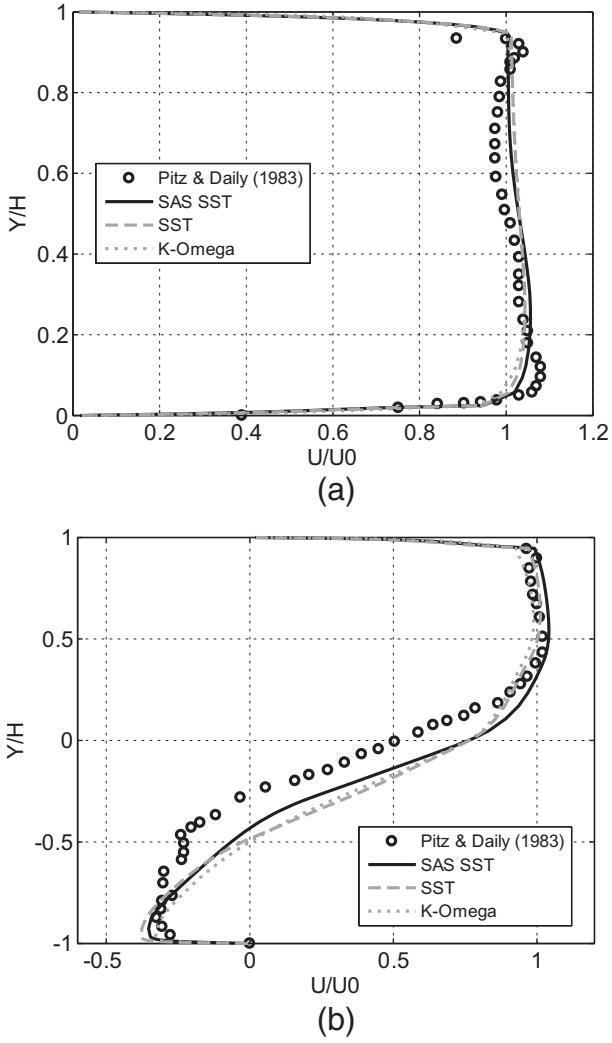

Fig. 3. Predicted velocity profile of Configuration 1 at (a) X/H = 0 (b) X/H = 3 for non-reacting flow ($\phi = 0$).

for the propane–air gas mixture. Based on the previous results for non-reacting flow, the SAS–SST model, which gives the best non-reacting flow prediction, is used to model the turbulence effects. Overall, one can say this model yields satisfactory results for the mean velocity profile of the reacting flow. Just behind the step at X/H = 1 the flow is almost stagnant and not very turbulent. In this location at the step height (i.e. Y/H = 0), there is a large velocity gradient while further downstream where the hot reactants are penetrating into the cold flow at the centre of the channel, velocity changes gradually. The maximum reverse velocity in the non-reacting flow at X/H = 3 was 0.31 U_0; while as seen in Fig. 4, in the reacting flow it is about 0.47 U0 meaning that the maximum reverse velocity in the reacting flow is higher which is due to the heat release. The important observation is that within the height of the step (Y/H < 0), the reverse velocity is underpredicted by the model pointing to the fact that the strength of

Table 2
Reattachment lengths calculated at $Re_h = 22000$ for non-reacting flow ($\phi = 0$).

	L/H	
	Present work	Error (%)
SAS SST	6.78	3.14
SST	6.67	4.71
$k-\omega$	6.54	6.57
Experiment [16]	7	–

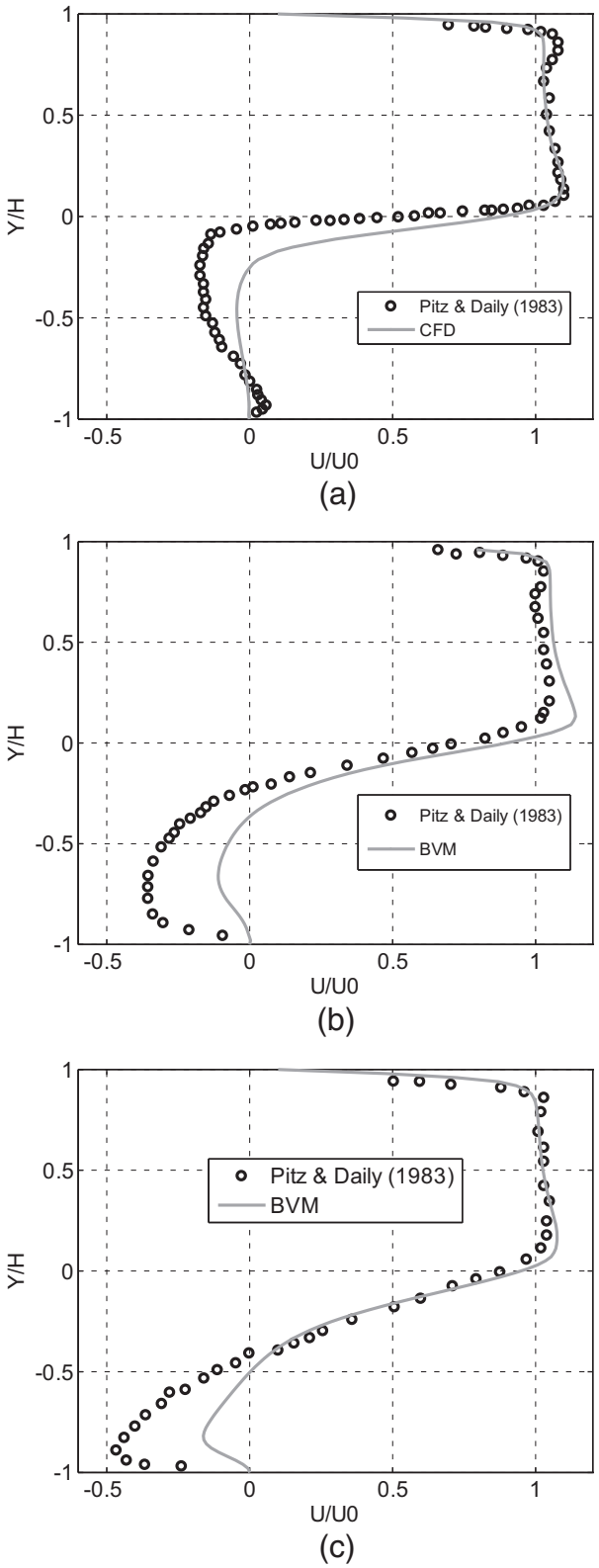

Fig. 4. Predicted stream-wise velocity profile in configuration 1 at (a) X/H = 1 (b) X/H = 2 (c) X/H = 3 for reacting flow ($\phi = 0.57$).

the predicted recirculation zone is less than the measurements. While above the step height (i.e. center channel), velocity profiles are in good agreement with the measurements. That can be explained due to the deviation from two-dimensional behavior which can affect the size and strength of the vortexes formed behind the step.

Table 3 shows reattachment lengths calculated for the reacting flow. Here, as a result of the expansion due to combustion, the reattachment length decreases 35% compared to the non-reacting flow (L/H = 7). In this case, the reattachment length is numerically predicted with an error about 2% which is fairly acceptable.

5.2. Configuration 2: backward facing step with heated wall

Due to the thermal interaction between hot gases and the colder liner wall, and also the correlation between gas temperature, density and speed of sound, correct prediction of the heat transfer is of high importance. The effects of the enhanced heat transfer between hot gases and the liner during the unstable regime of the combustor may result in damage of the liner where there is interaction between the flame and the wall. For this reason and to verify the accuracy of the models to predict the heat transfer, in this section simulations are done for the case of stationary flow across a backward facing step with a heat source embedded across the bottom wall downstream the step. Geometric details of the control volume and the coordinate system applied in this section follow the setup as used by Vogel et al. [17]; the length of the domain is 40 H, the height upstream and downstream of the step are respectively equal to 4 H and 5 H for an expansion ratio ER $= \frac{W}{(W-H)}$ of 1.25, while the value of H is taken as 3.8 cm. Similar to the configuration 1, the CFD domain in this configuration has a third dimension with a thickness equal to the size of one numerical element. Definition of the boundary condition relies on the properties of the physical condition known through the experimental data. Therefore, a constant heat flux, $q'' = 270\ W/m^2$ is embedded across the bottom wall, downstream of the step. To make a comparison in this case the Reynolds number (Re_h) is fixed to 28,000 and air at ambient temperature is selected as a working fluid. The chamber is subjected to an external air flow at room temperature entering the computational domain upstream of the step expanding downstream and forms a recirculation region as it is shown in Fig. 5. The velocity field at the inlet is specified as that of a fully-developed turbulent channel flow at a similar Reynolds number. However the reference free stream velocity is equal to 11.3 m/s. A pressure-based outlet boundary condition is used for the outflow. The other boundaries are considered as adiabatic and no-slip velocity boundary conditions. Based on the previous calculations done on the configuration 1, the SAS–SST model is chosen for modeling the turbulence effects.

According to Fig. 6, the main bulk of the flow field away from the wall was modeled fairly well. Velocity profiles showed good agreement with the experiments. The main differences are observed near the bottom wall, especially in vicinity of the centre of the recirculating zone. Here, the velocity gradients are under predicted. The reattachment length is predicted to be 6.8 H which gives an error of 1.9% compared to the measured value of 6.67 H. Generally velocity profiles demonstrate the growth of the shear layer, and the subsequent contact of flow with the wall at the reattachment point.

Fig. 7 shows the comparison of the temperature profiles at different streamwise positions downstream of the step. Significant gradients in the temperature are observed in the near wall region along the length of the downstream section. The only exception, (i.e. the only region far from the wall where significant temperature gradients occur) is

Table 3
Reattachment lengths calculated at $Re_h = 22000$ for reacting flow ($\phi = 0.57$).

	L/H		
	Present work	Experiment [16]	Error (%)
Reacting flow	4.4	4.5	2.2

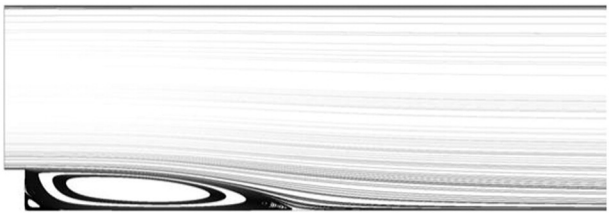

Fig. 5. Stream function of mean flow averaged in space.

immediately behind the step. This is due to the presence of the secondary bubble as well as the larger recirculating zone squeezing the induced flow. The spread of the mean temperature gradients downstream the reattachment location clearly shows the growth of the thermal boundary layer.

Fig. 8 compares the predicted and measured Stanton number (St); this dimensionless number represents the ratio of heat which is transferred into the fluid to the thermal capacity of the fluid, as:

$$St = \frac{h_c}{\rho u c_p} \tag{44}$$

where h_c is the convection heat transfer coefficient, equal to the ratio of heat flux (q″) to temperature difference between wall temperature (T_w) and external boundary temperature (T_0); ρ, c_p and u are the density, the specific heat and speed of the fluid, respectively.

According to Fig. 8, both Stanton number profiles show the same feature. The position of the maximal Stanton number peak and also the peak magnitude are precisely predicted which are in consistence with experiments. Keeping in mind that the location of X/H = 0 corresponds to the step location, it can be observed that the low heat transfer rate occurs in the recirculation region which is followed by a steep increase. The maximum value of Stanton number is achieved approximately slightly upstream of reattachment point which is equal to 6.8 H. Compared to Fig. 7, it can be concluded that the decrease in wall temperature (T–T0) is accompanied by an increase in convective heat transfer till its maximum value near the reattachment point, while downstream the reattachment the Stanton number decreases as the wall temperature is increased.

6. Conclusion

In this work, numerical investigation of turbulent flow with regions of separation behind a Back ward facing step have been carried out for both reacting and non-reacting flow. Among the investigated turbulence models ($k-\omega$, SST and SAS–SST), SAS–SST model showed the best agreement with the experimental data. The chosen turbulence model was used for the calculation of well documented case of turbulent flow over a back ward facing step with the heated wall, showing satisfactory results compared to experimental data. For modeling of the reacting flow, the BVM combustion model was used. The predicted results using this model showed accurate results with an error about 2% on prediction of reattachment length.

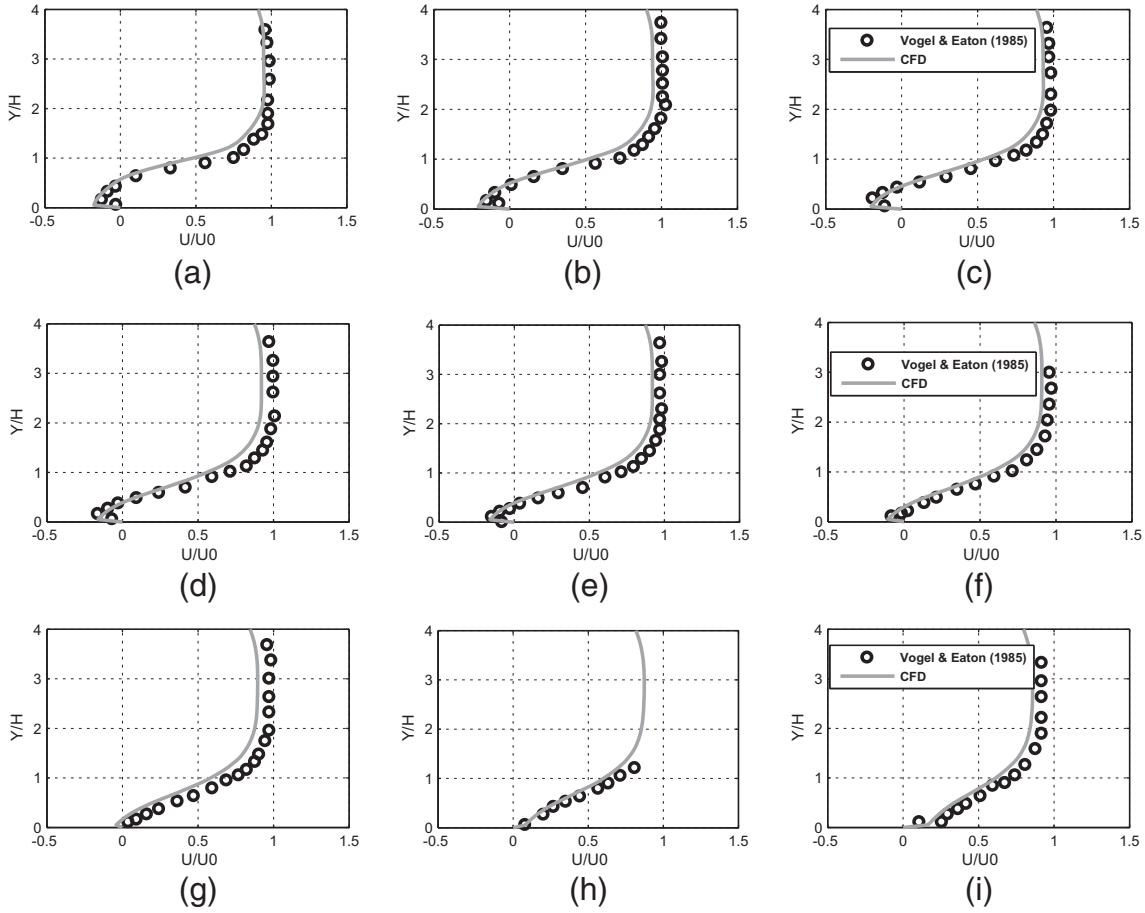

Fig. 6. Velocity profiles at various locations (a) X/H = 2.3, (b) X/H = 3, (c) X/H = 3.73, (d) X/H = 4.46, (e) X/H = 5.20, (f) X/H = 5.94, (g) X/H = 6.67, (h) X/H = 7.4, (i) X/H = 8.87.

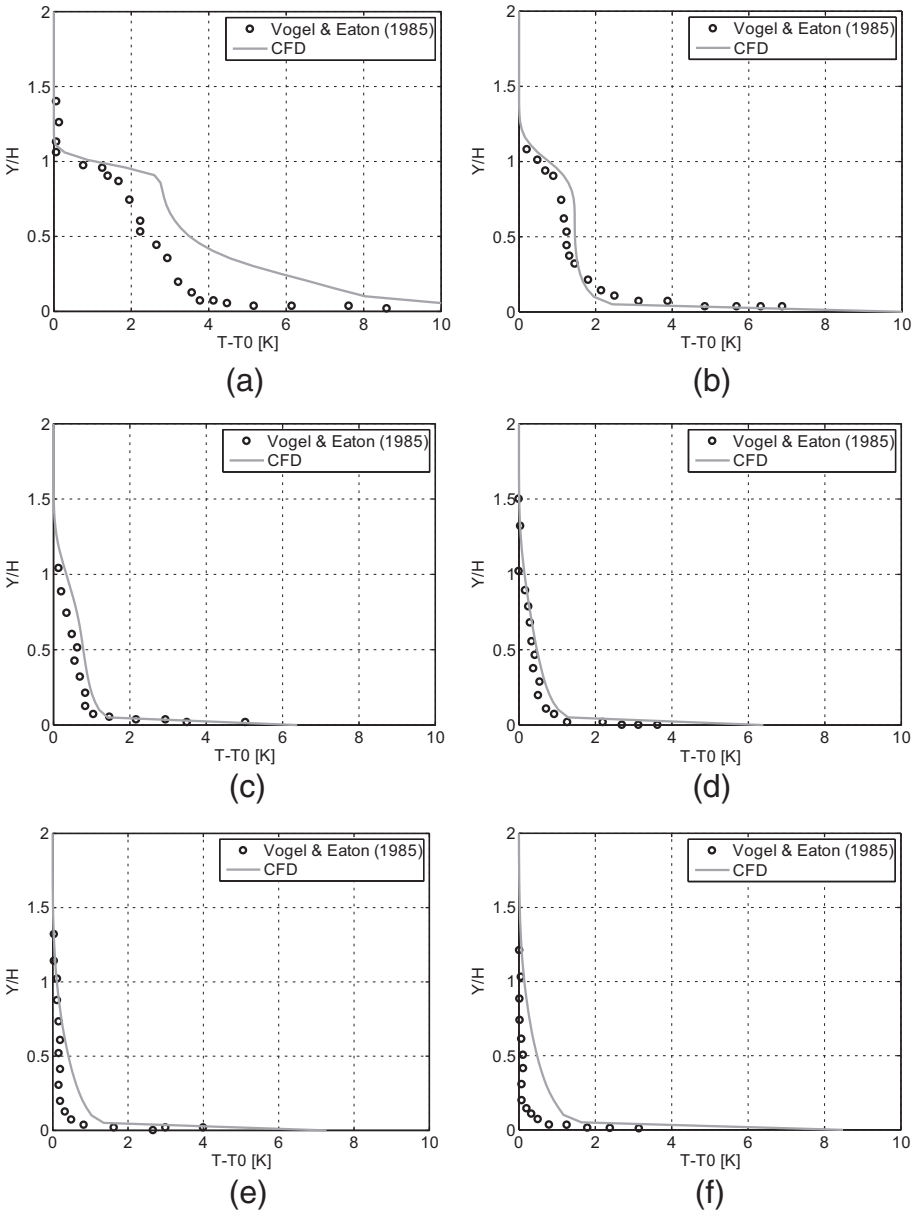

Fig. 7. Temperature profiles at different locations (a) X/H = 0.33, (b) X/H = 1.7, (c) X/H = 4.3, (d) X/H = 7, (e) X/H = 9.7, (f) X/H = 15.

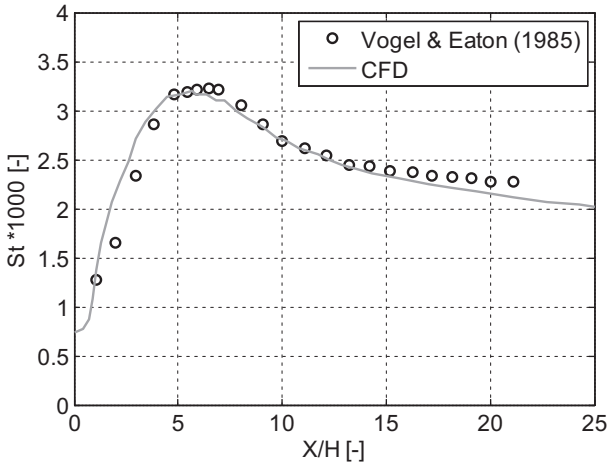

Fig. 8. Predicted and measured Stanton number along the bottom line of the BFS.

Acknowledgments

The authors would like to acknowledge the support of the EC in the Marie Curie Actions — Networks for Initial Training, under call FP7-PEOPLE-2007-1-1-ITN, Project LIMOUSINE with project number 214905.

References

[1] D.E. Abbott, S.J. Kline, Experimental investigation of subsonic turbulent flow over single and double backward facing steps, J. Basic Eng. 84 (1962) 317–325.
[2] E.W. Adams, J.P. Johnston, Effects of the separating shear layer on the reattachment flow structure part 2: reattachment length and wall shear stress, Exp. Fluids 6 (1988) 493–499.
[3] A. Valencia, Effect of pulsating inlet on the turbulent flow and heat transfer past a backward-facing step, Int. Commun. Heat Mass Transf. 24 (1997) 1009–1018.
[4] H.F. Oztop, K.S. Mushatet, İ. Yılmaz, Analysis of turbulent flow and heat transfer over a double forward facing step with obstacles, Int. Commun. Heat Mass Transf. 39 (2012) 1395–1403.
[5] I.I. Yılmaz, H.F. Öztop, Turbulence forced convection heat transfer over double forward facing step flow, Int. Commun. Heat Mass Transf. 33 (2006) 508–517.
[6] R. Friedrich, M. Arnal, Analysing turbulent backward-facing step flow with the lowpass-filtered Navier–Stokes equations, J. Wind Eng. Ind. Aerodyn. 35 (1990) 101–128.

[7] R.V.R. Avancha, R.H. Pletcher, Large eddy simulation of the turbulent flow past a backward-facing step with heat transfer and property variations, Int. J. Heat Fluid Flow 23 (2002) 601–614.
[8] B.F. Armaly, F. Durst, J.C.F. Pereira, B. Schönung, Experimental and theoretical investigation of backward-facing step flow, J. Fluid Mech. 127 (1983) 473–496.
[9] A.K. Pozarlik, J.B.W. Kok, Numerical simulation of a turbulent flow over a backward facing step with heated wall: effect of pulsating velocity and oscillating wall, J. Therm. Sci. Eng. Appl. 4 (2012) 041005.
[10] S.Y. Lee, S. Seo, J.C. Broda, S. Pal, R.J. Santoro, An experimental estimation of mean reaction rate and flame structure during combustion instability in a lean premixed gas turbine combustor, Proc. Combust. Inst. 28 (2000) 775–782.
[11] K.C. Schadow, E. Gutmark, Combustion instability related to vortex shedding in dump combustors and their passive control, Prog. Energy Combust. Sci. 18 (1992) 117–132.
[12] B. Emerson, J. O'Connor, M. Juniper, T. Lieuwen, Density ratio effects on reacting bluff-body flow field characteristics, J. Fluid Mech. 706 (2012) 219–250.
[13] S.J. Rees, Hydrodynamic Instability of Confined Jets & Wakes and Implications for Gas Turbine Fuel Injectors(Vol. PhD thesis) University of Cambridge, 2009.
[14] A.K. Pozarlik, Vibro-Acoustical Instabilities Induced by Combustion Dynamics in Gas Turbine Combustors(Vol. PhD) University of Twente, Enschede, The Netherlands, 2010.
[15] H.M. Altay, R.L. Speth, D.E. Hudgins, A.F. Ghoniem, Flame–vortex interaction driven combustion dynamics in a backward-facing step combustor, Combust. Flame 156 (2009) 1111–1125.
[16] R.W. Pitz, J.W. Daily, Experimental study of combustion in a turbulent free shear layer formed at a rearward facing step, AIAA J. 21 (1983) 1565–1570.
[17] J.C. Vogel, J.K. Eaton, Combined heat transfer and fluid dynamic measurements downstream of a backward-facing step, J. Heat Transf. 107 (1985) 922–929.
[18] G. Biswas, M. Breuer, F. Durst, Backward-facing step flows for various expansion ratios at low and moderate Reynolds numbers, J. Fluids Eng. 126 (2004) 362–374.
[19] T. Lee, D. Mateescu, Experimental and numerical investigation of 2-D backward-facing step flow, J. Fluids Struct. 12 (1998) 703–716.
[20] S.V. Patankar, Numerical Heat Transfer and Fluid Flow, Hemisphere, New York, 1980.
[21] L.Y.M. Gicquel, G. Staffelbach, T. Poinsot, Large Eddy simulations of gaseous flames in gas turbine combustion chambers, Prog. Energy Combust. Sci. 38 (2012) 782–817.
[22] H.K. Versteeg, W. Malalasekera, An Introduction to Computational Fluid Dynamics: The Finite Volume Method, Pearson Education Limited, 2007.
[23] D.C. Wilcox, Turbulence Modeling for CFD, 3rd ed. CW Industries, Inc., La Canada CA, 2006.
[24] D.C. Wilcox, Formulation of the k-omega turbulence model revisited, AIAA J. 46 (2008) 2823–2838.
[25] F.R. Menter, 2-Equation eddy-viscosity turbulence models for engineering applications, AIAA J. 32 (1994) 1598–1605.
[26] F.R. Menter, Y. Egorov, The scale-adaptive simulation method for unsteady turbulent flow predictions. Part 1: theory and model description, Flow Turbul. Combust. 85 (2010) 113–138.
[27] ANSYS, Combustion Theory, ANSYS CFX Release 11.0December 2006.
[28] V.L. Zimont, Gas premixed combustion at high turbulence. Turbulent flame closure combustion model, Exp. Thermal Fluid Sci. 21 (2000) 179–186.
[29] K. Bray, P. Domingo, L. Vervisch, Role of the progress variable in models for partially premixed turbulent combustion, Combust. Flame 141 (2005) 431–437.